Materials Horizons

Accepted Manuscript

This article can be cited before page numbers have been issued, to do this please use: F. Wang, S. Xiao, Y. Zhuo, W. Ding, J. He and Z. Zhang, *Mater. Horiz.*, 2019, DOI: 10.1039/C9MH00859D.

ROYAL SOCIETY OF CHEMISTRY

rsc.li/materials-horizons

Materials Horizons

View Article Online
DOI: 10.1039/C9MH00859D

COMMUNICATION

Liquid layer generator for excellent icephobicity at extremely low temperature

Received 00th January 20xx,
Accepted 00th January 20xx

DOI: 10.1039/x0xx00000x

Feng Wang[a], Senbo Xiao[a], Yizhi Zhuo[a], Wenwu Ding[b], Jianying He*[a] and Zhiliang Zhang*[a]

Progress in icephobicity has been made in recent years. However, the majority of the icephobic surfaces reported are relying on mechanisms of static nature, and maintaining low ice adhesion of these surfaces at extreme temperature as low as -60 ℃ is highly challenging. Dynamic anti-icing surfaces, that can melt ice at or change the ice-substrate interfaces from solid to liquid phase after the formation of ice serves as a viable alternative. In this study, liquid layer generators (LLGs), which can release ethanol to the ice-solid interface and convert ice-substrate contact from solid-solid to solid-liquid-solid mode were introduced. Excellent icephobicity on surfaces with an ethanol lubricating layer is found to withstand extremely low temperature (-60 ℃) by both molecular dynamic simulations and experiments. Two prototypes of LLG, one by packing ethanol inside and the other by storing replenishable ethanol below the substrate, are fabricated. The LLGs are able to constantly release ethanol for maximally 593 days without source replenishing. Both prototypes demonstrate super-low ice adhesion strength of 1.0~4.6 kPa and 2.2~2.8 kPa at -18 ℃. For selected samples, by introducing interfacial ethanol layer, ice adhesion strength on the same surfaces unprecedented decreased from 709.2~760.9 kPa to 22.1~25.2 kPa at low temperature of -60 ℃.

Conceptual insight

State-of-the-art icephobic surfaces mainly rely on static solid-solid ice-substrate contact, which fail at low temperature reaching a threshold of around -50°C. New strategy for anti-icing at such low temperature is missing. Dynamic anti-icing surfaces, which can melt ice at or change the ice-substrate interfaces from solid to liquid phase after the formation of ice serves as a viable alternative. In the current study, durable polymeric materials, termed liquid layer generators, were design and fabricated targeting low ice adhesion strength at unprecedentedly low temperature. The liquid layer generators were able to constantly release interfacial ethanol for maximally 593 days, which dynamically convert ice contact from firm solid-solid to weak solid-liquid-solid mode, and demonstrated super low ice adhesion strength of ~1 kPa. By introducing porous layer below substrate, interfacial liquid layer can be controlled by replenishable ethanol. The liquid layer generator can also overcome problems of surface roughness and hydrophilicity that fail other icephobic surfaces. At extremely low temperature of -60°C, the liquid layer generators maintained low ice adhesion strength (22.1~25.2 kPa), showing encouraging potential for practical arctic anti-icing utilization.

Introduction

Unwanted ice formation and accretion is a common threat to road safety, aircrafts, electrical transmission cables, wind turbines and many others[1–3], which requires a huge amount of energy input for traditional de-icing[4]. Consequently, designing and deploying materials and surfaces that can assist the removal of ice have received growing interests[5]. In the recent years, four main classes of ant-icing/icephobic surfaces have been developed. Firstly, the lotus-leaf effect inspired superhydrophobic surfaces can delay or prevent ice formation[6,7]. Unfortunately, such super-hydrophobic surfaces can result in higher water freezing rate than smooth surfaces in high humidity environment[8], and its hierarchical surface structure could enable mechanical interlocking with strong ice adhesion[9,10]. Secondly, the lubricant infused surfaces that can repel incoming water and lower ice adhesion strength[11,12]. For this type of icephobic surfaces, the depletion of the lubricants remains an unsolved problem especially in the icing/de-icing cycles[13,14]. Thirdly, the interfacial slippage surfaces that imbibe oil into silicon elastomer and show low ice adhesion strength[15–17]. However, the swelling of polymer in the

[a] NTNU Nanomechanical Lab, Department of Structural Engineering, Norwegian University of Science and Technology (NTNU), Richard Birkelands vei 1A, Trondheim 7491, Norway

Norway; *E-mail: jianying.he@ntnu.no; zhiliang.zhang@ntnu.no

[b] Department of Energy and Process Engineering, Norwegian University of Science and Technology (NTNU), Kolbjørn Hejes v 1B, Trondheim 7491, Norway

Electronic Supplementary Information (ESI) available. See DOI: 10.1039/x0xx00000x

oil may degrade the mechanical durability of this composite. Finally, the macro-crack initiators (MACI) and stress localization promoted surfaces that facilitate the crack generation through stiffness inhomogeneity and deformation incompatibility, and achieve super low ice adhesion strength without the use of any surface additives[18,19]. The MACI surfaces can combine with other mechanisms to further reduce ice adhesion. Notably, other new strategies for anti-icing are emerging, especially those consider ice growth and patterns into surface icephobicity designed[20,21,22].

The surfaces discussed above can be generally categorized as static anti-icing surfaces, meaning that there is no dynamic change of the chemical/physical state of the ice-substrate interfaces on these surfaces after ice formation. In contrast, emerging dynamic anti-icing strategies focus on melting or altering the solid ice-substrate interfaces[23,24]. One interesting example of these new dynamic anti-icing surfaces is the photothermal trap approach that utilizes solar illumination or near-infrared irradiation for rapid melting of the accumulated ice[23]. Another notable dynamic anti-icing surface contains polymers with hydrophilic pendant groups that can absorb water from ice and generate aqueous lubricating layer at the interface[21]. These dynamic anti-icing surfaces hold the potential of gradually converting firm solid-solid ice-substrate contacts to a weak solid-liquid-solid manner, and could maintain icephobicity in a broad temperature range[24]. For instance, the photothermal trap can result in a temperature rise as high as 33°C[23], and the aqueous lubricating layer shows great icephobicity before -53°C[24].

The ice adhesion strength on the dynamic anti-icing surfaces with an aqueous lubrication layer was reported to be ~27 kPa[24], which await optimization to achieve practical passive anti-icing application level (lower than ~12 kPa)[18,25]. The icephobicity of the dynamic anti-icing surface relies critically on generating an interfacial aqueous layer. When this crucial interfacial liquid layer froze at low temperature, for instance close to -60 ℃, ice adhesion strength can sharply increase to higher than 400 kPa[24]. Thus, the ability of dynamic anti-icing surfaces to maintain icephobicity in arctic environment with extreme low temperature of -60 ℃ or even lower is still a big challenge.

The aim of this work is to realize dynamic icephobic surfaces that can function at extreme low temperature. We focused on fabricating coating, termed liquid layer generator (LLG), which can release ethanol at the ice-solid interface for generating lubricating effect and yielding low ice adhesion strength. We first used atomistic modeling and simulations to compare ice adhesion force on substrates with and without a liquid lubricating layer at various temperature down to -60 ℃, and probed the reduction of atomistic ice adhesion by substituting the interfacial aqueous layer to a lubricating ethanol layer. On such theoretical basis, we synthesized ethanol-contained polymer with various roughness and chemical components that can release ethanol to the ice-substrate interface, namely generating interfacial liquid layer. The fabricated LLGs were found to function at -60 ℃ with promising icephobicity and significant lifespans. Our combined theoretical and experimental study contributes to the novel dynamic anti-icing field. The LLGs can provide a path to push forward anti-icing applications to unprecedentedly low temperature.

Materials and methods

Atomistic modelling and Molecular dynamics (MD) simulations

Atomistic modeling and MD simulations were employed to investigate the lubricating effect of an ethanol layer with various thickness at different temperature. For the sake of simplicity, graphene platelets in dimension of 2.3 nm × 2.3 nm were used to build a carbon-based surface, as shown in Supplementary Fig. S1. The graphene platelets stacked on each other in equilibrium distance at each edge of ~0.6 nm, and extended a periodic area of 10.4 nm × 10.4 nm. Ice with thickness of 2 nm with and without ethanol layers of 1 and 2 nm, was then modeled on the substrate, as example system snapshots shown in Fig. S1a and Supplementary Fig. S2. A simulation system with an interfacial aqueous layer of 2 nm in thickness was also built for comparing lubricating effect, as shown in supplementary Fig. S3(a). The water molecules used the tip4p/ice model in this system. The OPLS force field was used for the graphene platelets and the ethanol layer, and the tip4p/ice model was used for the ice in all the MD simulations[26,27]. The MD package, GROMACS 5.0.7, was employed to carry out all the simulations[28]. All the systems were equilibrated for 50 ns before subjected to probe ice adhesion and shearing simulations. In all (MD) simulations, the time step used was 2 fs. The cut-off of non-bonded interaction was 1 nm. The graphene platelets were completely fixed at their position, providing a solid surface. The ice was maintained at a temperature of -93 ℃ similar to a former study[29]. The ethanol layers were kept at various temperatures of -18 ℃, -35 ℃ and -60 ℃ in different simulations. The same simulation parameters were applied to the system with aqueous lubricating layer for comparing lubricating effect at these three temperatures. The temperature coupling method Nosé-Hoover was employed in the simulations[30,31], with coupling constant of 0.4 ps. In order to obtain the ice adhesion strength and shearing stress, pulling force was acting on the center-of-mass (COM) of the ice similar to former studies[29,32]. The force constant of the pulling harmonic potential was 500 kJ/mol/nm^2 in probing the vertical ice adhesion strength. Because of the limited space in shearing horizontally in the periodic simulation box, the harmonic potential was 2000 kJ/mol/nm^2. The pulling speed in all the de-icing simulations was 0.5 m/s. The ice adhesion strength was calculated using the maximal force in vertical pulling normalized by the surface cross-section area, namely $\sigma = f_{max}/A$, while the ice shearing stress was obtained by the shearing force normalized by the surface cross-section area, $\tau = f_{shear}/A$.

Fabrication of LLGs with ethanol inside the substrates

We used silicon rubber Ecoflex^{TM} 00-50 (Smooth-On, Inc.) as matrix material. The silicon rubber was added in two steps. The silicon rubber part A was first mixed with absolute ethanol (Sigma-Aldrich) by mechanical stirring for 3min. The part B was added immediately, and the whole mixture was stirred for another 3 min. The ethanol content in the mixture were 10, 20, 30, 40 vol%, respectively. The final mixtures were casted into plastic molds and cured at room temperature. After 3 hours, LLG 1 with various ethanol content were fabricated. The ethanol droplets initially trapped in the silicon rubber were spherical as indicated by Supplementary Fig. S4, with diameter ranged from 0.37 to 0.47 mm depending on the ethanol volume content (Supplementary Fig. S5). The ethanol droplets formed in the silicone rubber curing process, which mostly resulted from the exclusion of the ethanol molecules by the cured polymer chains. The ethanol droplets were thus firmly imprisoned in the polymer matrix at the initial state of the LLG 1.

Fabrication of LLGs with capacity below substrates for replenishable ethanol

Firstly, 4-inch silicon wafers were cleaned successively with ethanol, acetone and isopropanol. Then, mr-DWL 5 (Micro resist technology GmbH) was spin-coated on the silicon wafer at 2000 rmp for 30 s, followed by prebaking at 50 and 90 °C (5 min for each). The silicon wafer with mr-DWL5 was exposed with MLA150 (Maskless Photolithography MLA-150, Heidelberg Instruments), followed by post baking at 50 and 90°C (5min for each). After developed in mr-Dev 600 (Micro resist technology GmbH) for ~35 min and hard baked at 150 °C for 15 min, silicon wafer with pillars of uniform size were fabricated. The patterned area was controlled 5 cm × 5 cm for all wafers. The distance between the pillars varied from 5 μm to 30 μm as shown in Fig. 4a-c and supplementary Fig. S8.

The silicon wafers with pillars were silanized with trichloro(1H,1H,2H,2H-perfluoroocty)silane (Sigma-Aldrich) in a vacuum chamber for 8h to make it easier for PDMS peeling off. PDMS prepolymer (Sylgard 184, Dow Corning) and curing agent were mixed in a weight ratio of 10:1 and stirred for 5 min. The mixtures were degassed in a vacuum chamber for 30 min to remove air bubbles. The liquid was poured on to patterned silicon wafer and held for 5 min, and then spin-coated (WS-400B-6NPP-LITE/AS, Laurell Technologies) for 1 min at a speed of 500 rpm to obtain PDMS film with thickness of 420 μm. After cured at 60 °C for 3 h, PDMS films with sub-holes were carefully peeled off from the silicon substrates. The films were transferred to glass and ready for the ice adhesion tests. To finalize the LLG 2, ethanol was filled into the sub-pores using injector.

Silica nanoparticles and PVA were used as surface modifiers of PDMS surfaces. SiO_2 were synthesized through a facile method. Firstly, 5 ml ammonium hydroxide (28%, Sigma-Aldrich), 95 ml absolute ethanol (>99.8%, Sigma- Aldrich) and 5ml deionized water were mixed and stirred in a three-necked flask for 10 min. Secondly. The mixture was heated to 60 °C, and then 3 ml tetraethyl orthosilicate (TEOS, >99.8%, Sigma-Aldrich) was added. Finally, after stirring for another 12 h, the ethanoic suspension of silica nanoparticles with particle size ~222.7 nm were obtained (the particle size distribution was shown in supplementary Fig. S9). The as-prepared suspension was dripped onto PDMS surfaces and spin-coated for 30 s at a speed of 800 rpm, which was repeated for five times. Poly(vinyl alcohol) (PVA, fully hydrolyzed, Sigma-Aldrich) was dissolved in water under 100 °C to obtain a clear solution of 3 wt%. The as-prepared solution was dripped onto PDMS surfaces and spin-coated for 30 s at a speed of 800 rpm, which was also repeated for five times. The modified films were heated at 60 °C for 3 h to finalize the treating of the PDMS films. To obtain LLG, ethanol was filled into the sub-pores using injector.

Characterizations

Chemical structures of the liquid layer at the ice-substrate interface were examined by NMR (Bruker Avance III 400 MHz). Surface morphologies were observed by the field emission scanning electron microscope (FEI APREO SEM). All samples were sputter-coated with a 5 nm gold layer. Microscopy photos of silicon wafers with different patterns were taken by DIC microscope (Zeiss AxioScope A1 for Reflected light BF-DIC/POL, Carl Zeiss). The surface morphology of the coatings was recorded by atomic force microscopy (AFM, Veeco Metrology) using Peak Force Quantitative Nano-Mechanics mode. Ice adhesion strength was measured by a universal mechanical tester (Instron Model 5944) equipped with lab-built cooling system and chamber, as described in previous studies[18]. A polypropylene centrifuge tube with a 1 mm thick wall and a 20 mm inner diameter was placed onto the coatings. 1.5 mL deionized water was infused into each mold, the samples were placed in a freezer with constant temperature of -18 °C for 3 hours to ensure complete freezing. Before test, the samples were transferred from the freezer to the cooling chamber of the test machine. For the test at -18 °C, the samples were stabilized in the cooling chamber of the test machine at -18 °C for 10 min before tested. For the test at -60 °C, the samples were stabilized in the cooling chamber of the test machine at -60 °C for 1 h to ensure total cool before tested. During ice adhesion test, a force probe with 5 mm diameter propelled the tube-encased ice columns at a velocity of 0.01 $mm \cdot s^{-1}$, and the probe was located close to the tested coating surface (less than 1 mm) to minimize the torque on the ice cylinders. The loading curve was recorded, and the peak value of the shear force was divided by contact area to obtain the ice adhesion strength. Four samples from each composition were measured to obtain the mean ice adhesion strength.

Results and discussion

Lubricating effect of a nanoscale interfacial ethanol layer

The purpose of atomistic modeling and simulations was to verify the lubrication effect of an ethanol layer at the ice-solid interface at various temperature. Simulation systems with and without interfacial ethanol layers on a model carbon-base substrate were built for this purpose, as shown in Fig. 1 and supplementary Fig. S1 and S2. Pulling force was utilized to probe atomistic ice adhesion strength in the systems, with details given in the Methods Section.

A layer of lubricating ethanol can indeed greatly reduce atomistic

ice adhesion strength (σ) and shearing stress (τ). As depicted in Fig. 1a, ice adhesion strength was defined as the highest stress needed to vertically detach the ice from the substrate, while shearing stress was monitored in the horizontal shearing process using shearing force normalized by the surface area. Without an ethanol layer, the ice adhesion strength obtained in 5 independent simulations was 351±4 MPa. In comparison, a sandwiched ethanol layer of 1 nm reduced the ice adhesion strength down to 160±3 MPa, showing a drastic reduction over ≥50%. When the ethanol layer was 2 nm in thickness, ice adhesion strength was further reduced to 83±2 MPa, which was another ~50% reduction. This result not only confirmed the icephobic potential of a lubricating ethanol layer and its thickness effect, but also showed the accumulation of ethanol, from 1 to 2 nm, at the ice-solid interface was highly beneficial for de-icing operation.

The lubrication effect of the ethanol layer was also significant, and reduced ice shearing stress with increasing layer thickness at extremely low temperature. As shown in Fig. 1c, without a lubricating layer, the ice shearing stress profile was in typical stick-slip pattern similar to former studies[33,34], showing an initial stress peak values exceeding 85 MPa. Such high peak values indicated the high stress needed to initiate ice cracking during de-icing. In comparison, an interfacial ethanol layer with thickness of 1 nm effectively smoothed the shearing stress profile and yielded average shearing stress of 34.5±4.5 MPa at -18°C. When the ethanol layer thickness was 2 nm, the ice shearing stress further reduced to 7.8±1.4 MPa. The lubricating effects of the ethanol layer held at even lower temperature, as indicated in Fig. 1d. When the temperature decreased from -18 °C to -38 °C, the ice shearing stress obtained with the ethanol layer of 2 nm increased to 20.6±2.7 MPa. At extremely low temperature of -60 °C, the ice shearing stress further increased to 33.2±4.8 MPa. All the ice shearing stress profiles obtained at various temperature showed smoothening effects of the ethanol layer, and average values lower than the peak values of shearing ice without an ethanol layer, which suggested that generating an ethanol layer at the ice-solid interface could facilitate de-icing at low temperature. The lubricating effect of an ethanol layer was outperforming an aqueous layer. As shown in Fig. S3 in supplementary information, ice shearing stress with an aqueous layer of 2 nm in thickness exhibited much higher value than with ethanol layer shown in Fig. 1d at -18 °C and -38 °C. The aqueous layer lost lubricating effect completely at -60 °C, confirming former study results of deficiency of the aqueous layer in low temperature anti-icing applications[24]. It should be noted that the loading rate used in the simulations is orders of magnitude higher than in the experiment, which results in much higher absolute ice adhesion strength values[35]. Yet the difference in ice adhesion mechanics is significant under the same simulation parameters and protocol.

Design principles and fabrication of icephobic LLG

The atomistic modeling and simulation results above indicated that an ethanol layer with increasing thickness at the ice-substrate interface could greatly reduce ice adhesion strength. Most importantly, the lubricating effect and thus surface icephobicity by such interfacial ethanol layer could function at temperature as low as -60 °C as ethanol has low freezing point of -115 °C. The experiments were devoted to design the LLG that could dynamically accumulate ethanol molecules to form a lubricating layer between substrate and ice. Two strategies were chosen for fabricating LLGs as depicted in Fig. 2a, namely 1) packing ethanol inside the substrate (LLG 1) and 2) storing replenishable ethanol below the substrate (LLG 2). For LLG 1, ethanol was directly mixed into polymer substrate during synthesis process. In contrast, lamellar structures with sub-pores were created under the substrate for LLG 2, which allowed ethanol to be readily refilled after synthesis.

The icephobic mechanism of the LLG was shown in Fig. 2b. It was essential that LLG was able to release ethanol to the ice-substrate interface to generate an ethanol layer, as the quasi-liquid/liquid layer was the key for the low ice adhesion strength[24]. By taking into account that ethanol could absorb onto ice surface for creating quasi-liquid/liquid layer[36,37], and elastomer membranes were preferential for ethanol permeation[38,39], silicon rubbers were chosen as the matrix material for fabricating the two LLG substrates. One can see that with such design principle and material selection, ethanol molecules inside or below the LLG could dynamically permeate through the polymer matrix and reach the ice-substrate interface. It was expected that the accumulated interfacial ethanol would finally create a liquid layer that convert ice-substrate contact from firm solid-solid to weak solid-liquid-solid mode. The fabrication procedures of the two LLGs were briefly shown in Fig. 2c-d, with experimental details given in the Materials and Methods section. Samples with serial of ethanol contents were fabricated and characterized for two LLGs, and were then subjected to icephobicity investigation.

Icephobicity of the LLGs with ethanol inside the substrate

The LLG 1 was fabricated through a facile synthesis method shown in Fig. 2c. Ethanol with different volume content (10~40%) were mixed with silicone rubber that could be quickly cured before a significant evaporation of ethanol. The thickness of the substrate was controlled at ~2 mm. The morphology and size distribution of ethanol droplets in the LLG 1 were shown in Fig. S4 and Fig. S5 in supplementary information. The LLG 1 indeed released ethanol to the interface and demonstrated excellent icephobicity. As exemplified by LLG 1 with 20vol% ethanol, ice cube on the LLG 1 surface spontaneously fell off in 3 hours after vertical placement (Fig. 3a). A liquid layer was detected after ice cube detached form LLG 1. As shown in Fig. 3b, visible dyestuff diffused on the ice cube peeled off from LLG 1 was observed, which confirmed the secretion of ethanol by the LLG 1. The liquid layer on the detached ice cube was carefully collected and transferred to ^{1}H NMR spectroscopy. As shown in the lower panel of Fig. 4b, the strong signal at 4.80 ppm was resulted from -OH of both ethanol and water, and the signal by -CH_2 and -CH_3 of ethanol were also clearly detected. Thus, the results from the ^{1}H NMR agreed with the structure of ethanol (CH_3CH_2OH). The ^{1}H NMR spectra confirmed the ethanol component in the liquid layer, which proved the ability of LLG 1 to release ethanol to ice-substrate interface.

Ice adhesion strength on the LLG 1 falls in the super-low region[18]. As shown in Fig. 3c, ice adhesion strength on LLG 1 ranged from 1.0 to 4.6 kPa, showing a steady decrease with increase content of ethanol in the substrate, all of which were lower than the same sample after ethanol exhaustion (8.6~10.0 kPa). It should be noted that the ice adhesion strength on smooth pure silicon rubber was 7.2 kPa, which was lower than that on the rough LLG 1 after ethanol exhaustion. Details of the roughness formation on LLG 1 surface was given in the Supplementary Materials Fig. S6. The thicker the interfacial ethanol layer, the lower ice adhesion strength, as confirmed by the atomistic modeling results above. LLG 1 with higher ethanol content could release more ethanol to the ice-substrate interface, thus thicker interfacial liquid layer, in the same given time, which account for the results shown in Fig. 3c (light blue curve). Such low ice adhesion strength is also lower than value obtained on pure silicon rubber (detailed comparison and discussion were given in the supplementary information). These results again verified the function of ethanol layer in enhancing icephobicity of surfaces.

The ethanol release rate underlies the icephobic durability of the LLG samples, and thus the lifespan of the LLGs. In order to evaluate the time needed for fully exhausting ethanol from the samples, the mass weight of LLG 1 in room temperature and -20 °C was tracked as functions of holding time after synthesis. At room temperature, the ethanol in LLG 1 would completely run out in 15 days, as shown in Fig. 3d. The weight loss of LLG 1 was lower than the initially ethanol content. This was because the curing process of LLG 1 took 3 hours. During this time, certain amount of ethanol evaporated, which was not taken into account in Fig. 3d. Surprisingly, releasing of ethanol from the LLG 1 kept at temperature of -20 °C could still be steadily observed after 250 days (Fig. S7). The release of ethanol molecules to the solid-ice interface was a spontaneous thermodynamics process. Because the freezing temperature of ethanol was extremely low, this spontaneous release can occur at a wide temperature range. There were multiple determinants of ethanol release rate, including diffusion efficiency of ethanol in the polymer, vapor pressure, temperature, their coupling and others[38]. The lower the temperature, the poorer ethanol release efficiency and longer life time of the LLG. The dynamics of ethanol release from the LLG 1 was analyzed and shown in supplementary Fig. S7, with detailed discussion. The icephobic lifetime of the LLG 1 was expected to be ≥250 days at a temperature of -20 °C, and was even longer at lower temperature. Especially, for the LLG 1 with 40 vol% ethanol, it was predicted to have a lifespan long to 593 days (Fig. S7). It was thus reasonable to anticipate long-term icephobicity of the LLGs at low temperature as long as the interfacial ethanol layer is not frozen.

Icephobicity of the LLGs with replenishable ethanol below the substrate

The LLG 1 well approved the ability of releasing ethanol to ice-substrate surface and achieved excellent icephobicity. By embedding a fix amount of ethanol inside the substrate, the LLG 1 was yet doomed to icephobicity depletion with the exhaustion of ethanol, despite the ≥250 days lifetime observed. The LLG 2 thus designed to extend the durability with capacity for easily replenishable ethanol, namely creating a lamellar structure with porous layer below the substrate, as depicted in Fig. 2d. For the sake of mechanical robustness, the polydimethylsiloxane (PDMS) with same silicone base as silicon rubber was for LLG 2, as it is one the commonly option for fabrication icephobic coatings[17-19,40-42]. Specifically, silicon wafers with pillars were used as templates for molding PDMS, as an example shown in supplementary Fig. S8. All the pillars have a fix radius of 5μm, with inter-pillar distance varied from 15μm to 30μm as shown in Fig. 4a-c, which led to complementing holes in the substrate for holding replenishing ethanol (Fig. 4d-f).

The LLG 2 with ethanol replenishing capacity shown equally low ice adhesion strength. As shown in Fig. 4g, the ice cube on LLG 2 spontaneously fell off in 3 hours at a temperature of -18 °C, while its counterpart adhered firmly on the sample without storing ethanol in the holes. The ice adhesion strength obtained on the LLG 2 with different holes density fell in the range of 2.2~2.8 kPa as shown in Fig. 4h, which decreased significantly comparing to the same surface without ethanol layer (47.3~86.7 kPa). After detachment of the ice cube from the LLGs, visible liquid droplets were detected on the surface (Fig. 4i), which evidenced the same mechanism of LLG shown in Fig. 2b. With the holes in the substrate and the ethanol replenishing capacity, the extended durability of LLGs was expected, which could guarantee long-term practical anti-icing applications.

Further verification and extremely low temperature applications of LLGs

The icephobic basis of LLGs is to generate a liquid ethanol layer at the ice-substrate interface, and converting ice contact from strong solid-solid to weak solid-liquid-solid mode. As long as continuing ethanol release from the substrates, surface roughness (possibly impurity) and chemistry should not hamper the functionality of LLGs. The LLG 2 was chosen to further verify the icephobicity of LLGs with altered surface roughness and chemistry. SiO_2 nanoparticles and hydrophilic polyvinyl alcohol (PVA) were used to coat the intrinsically hydrophobic PDMS LLG 2 for altering surface roughness and hydrophobicity separately. The nanoparticles had a mean diameter of 222.7 nm, with size distribution shown in supplementary Fig. S9, which led to surface topography of the treated LLG 2 shown in Fig 5a. The PVA coating on the LLG 2 had a thickness of 10 μm, as shown in Fig. 5b. The roughness of LLG 2 with and without surface treatment were investigated in Fig. S10 in supplementary information.

Notably, the ice adhesion strength on the treated surfaces showed encouraging results. By introducing roughness and hydrophilicity to the PDMS samples, ice adhesion strength significantly raised from 47.3~86.7 kPa (Fig. 4h) to 151.0~164.9 kPa (Fig. 5c) and 198.6~298.7 kPa (Fig. 5d), respectively. Such results were also in agreement with former studies that an increase of surface roughness and hydrophilicity led to higher ice adhesion strength[8,18,43]. By infusing ethanol into sub-holes, after 3 hours, icephobicity of the treated surface restored. As shown in

View Article Online
DOI: 10.1039/C9MH00859D

Fig. 5c-d, ice adhesion strength on LLG 2 coated with nanoparticle and PVA drastically decrease to 9.3~13.3 kPa and 10.8~12.4 kPa, respectively. The nanostructures and coatings on the LLG surfaces can hinder the lubricant release rate[44]. The ethanol release efficiency to the solid-ice interfaces was temperature dependent, namely faster releasing at higher temperature. The results suggested that the LLG functioned well on surfaces with different chemical components (both hydrophobic and hydrophilic surfaces) and on surfaces with different morphologies (both smooth and rough surfaces), demonstrating anti-icing potential in different application conditions.

It was known that both the properties of ice, its adhering surfaces and their interaction changed obviously as temperature went down, which led to significant increase in ice adhesion strength[45]. It was observed that ice adhesion strength increased roughly two orders of magnitudes, from ~55 to ~1156 kPa, when temperature decreased from -15 to -30 ℃[46]. The LLG could benefit from the low freezing point of ethanol, and the interfacial ethanol layer could maintain solid-liquid-solid ice contact at very low temperature. As simulation results shown in Fig. 1c-d and supplementary Fig. S3, the lubricating effect by ethanol can still act at a temperature of -60 ℃. Ice adhesion test at such low temperature were also carried out. Strikingly, ice adhesion strength on LLG 2 maintained at low value at -60 ℃. As results shown in Fig. 5e-f, after holding for 4 hours (3 hours in -18 ℃ and 1 hour in -60 ℃), both nanoparticle and PVA coated PDMS samples demonstrated high ice adhesion strength of 576.1~740.2 kPa and 709.2~760.9 kPa, respectively, while the counterpart LLGs shown low ice adhesion strength of 20.1~23.9 kPa and 22.1~25.2 kPa. It should be noted that lower ice adhesion on the LLGs could be expected for longer holding time, as more ethanol and thicker interfacial liquid layer can be generated by the LLGs. Comparing to former experimental studies where sharp increase in ice adhesion strength observed at -53 ℃[24], the LLGs approach was an outperforming dynamics icephobic/anti-icing strategy. Furthermore, considering the low freezing point of ethanol of -114.1℃, and a vast co-existing space of liquid ethanol and ice/water (lowest to -124 ℃ observed in experiments) shown in a phase diagram in supplementary Fig. S10[47–49], the liquid layer created by the LLGs is possible to function at a broad temperature range including in the extremely cold arctic environments.

Conclusion

In summary, this work introduced the liquid layer generator (LLG), which dynamically secreted a lubricating ethanol layer at the ice-solid interface after ice formation for low ice adhesion strength. Firstly, atomistic modeling and simulations were employed to depict the ice adhesion reduction effect of ethanol layers with different thickness at the ice-solid interface at various temperature. Fabrication of LLGs and ice adhesion test experiments of the LLGs were then carried out. Both the two LLGs prototypes, namely embedding ethanol in the substrate and storing replenishable ethanol in holding capacities, shew excellent icephobicity with lowest ice adhesion of 1.0 kPa observed at -18 ℃, which verified the function of ethanol layer generated by the design of LLG. Owing to the ability of constantly ethanol release and thickening of the interfacial lubricating layers, the LLG was able to overcome the deficiency effect by surface roughness and hydrophilicity, two critical factors failing many icephobic surfaces. The lifespan of the icephobicity of the LLGs was highly encouraging, especially with the replenishable ethanol. Most importantly, the LLG functioned well at low temperature covering the arctic anti-icing requirement, which outperformed other state-of-the-art icephobic surfaces. For the selected samples, by introducing interfacial ethanol layer, ice adhesion strength on the same surfaces unprecedented decreased from 709.2~760.9 kPa to 22.1~25.2 kPa at low temperature of -60 ℃. All these properties enable LLGs to be a competitive candidate for practical anti-icing applications and provide an icephobic solution for extremely low temperature that fail other former published icephobic surfaces.

Conflicts of interest

There are no conflicts to declare.

Acknowledgements

The Research Council of Norway is acknowledged for the support to the FRINATEK project Towards Design of Super-Low Ice Adhesion Surfaces (SLICE, 250990), and the PETROMAKS 2 project Durable Arctic Icephobic Materials (AIM, 255507) The computational resources were provided by the Norwegian Metacenter for Computational Science (NOTUR NN9110 and NN9391K)

References

1 A. K. Andersson and L. Chapman, UK. Accident Analysis & Prevention, 2011, 43, 284–289.
2 Gent R W, Dart N P, Cansdale J T. Philosophical Transactions of the Royal Society of London. Series A: Mathematical, Physical and Engineering Sciences, 2000, 358, 2873-2911.
3 U. Björnstig et al., Accident Analysis & Prevention, 1997, 29, 211–215.
4 J. L. Laforte et al., Atmospheric Research, 1998, 46, 143–158.
5 M. J. Kreder et al., Nature Reviews Materials, 2016, 1, 15003.
6 J. C. Bird, R. Dhiman, H. M. Kwon and K. K. Varanasi, Nature, 2013, 503, 385.
7 A. J. Meuler et al., ACS nano, 2010, 4, 7048–7052.
8 S. Jung et al., Langmuir, 2011, 27, 3059–3066.
9 A. J. Meuler et al., ACS applied materials & interfaces, 2010, 2, 3100–3110.
10 K. K. Varanasi et al., Applied Physics Letters, 2010, 97, 234102.
11 T. S. Wong et al., Nature, 2011, 477, 443–447.
12 P. Kim et al., ACS nano, 2012, 6, 6569–6577.
13 J. S. Wexler et al., Physical review letters, 2015, 114, 168301.

14 K. Rykaczewski et al., Langmuir, 2013, 29, 5230–5238.
15 K. Golovin et al., Science advances, 2016, 2, 1501496.
16 C. Urata et al., Journal of Materials Chemistry A, 2015, 3, 12626–12630.
17 K. Golovin et al., Science, 2019, 364, 371-375
18 Z. He et al., Soft matter, 2017, 13, 6562–6568.
19 Irajizad P, Al-Bayati A, et al. Materials Horizons, 2019, 6, 758-766.
20 Liu J, Zhu C, Liu K, et al. Proceedings of the National Academy of Sciences, 2017, 114 11285-11290.
21 Ahmadi S F, Nath S, Iliff G J, et al. ACS applied materials & interfaces, 2018, 10, 32874-32884.
22 Lin C, Corem G, Godsi O, et al. Journal of American Chemical Society, 2018, 140, 15804-15811.
23 S. Dash et al., Science advances, 2018, 4, 0127.
24 R. Dou et al., ACS applied materials & interfaces, 2014, 6, 6998–7003.
25 K. Golovin et al., Science advances, 2017, 3, 1701617.
26 W. L. Jorgensen et al., Journal of the American Chemical Society, 1996, 118, 11225–11236.
27 J. L. F. Abascal et al., The Journal of Chemical Physics, 2005, 122, 234511.
28 M. J. Abraham et al., SoftwareX, 2015, 1, 19–25.
29 S. Xiao et al., Nanoscale, 2016, 8, 14625–14632.
30 S. Nosé, The Journal of Chemical Physics, 1984, 81, 511–519.
31 W. G. Hoover, Physical review A, 1985, 31, 1695.
32 S. Xiao et al., Physical Chemistry Chemical Physics, 2018, 20, 24759–24767.
33 M. Beeman et al., Journal of Geophysical Research: Solid Earch, 1988, 93, 7625–7633.
34 J. R. Blackford et al., Faraday discussion, 2012, 156, 243–254.
35 Xiao S, Stacklies W, Cetinkaya M, et al., Biophysical journal, 2009, 96, 3997-4005.
36 C. Thierfelder et al., Physical Review B, 2007, 76,195426
37 J. P. D. Abbatt et al., Environmental Research Letters, 2008, 3, 045008.
38 H. O. Karlsson et al., Jornal of Membrane Science, 1993, 76, 121–146.
39 Li L, Xiao Z, Tan S, et al. Journal of Membrane Science, 2004, 243, 177-187.
40 F. Wang et al., Chemical Engineering Journal, 2019, 360, 243–249.
41 Y. Zhuo et al., ACS applied materials & interfaces, 2018, 10, 11972–11978.
42 Y. Zhuo et al., ACS Omega, 2018, 3, 10139–10144.
43 V. F. Petrenko et al., Canadian Journal of Physics, 2003, 81, 387–393.
44 Preston D J, Song Y, Lu Z, et al. ACS applied materials & interfaces, 2017, 9, 42383-42392.
45 H. H. G. Jellinek, Canadian Journal of Physics, 1962, 40, 1294–1309.
46 J. Chen et al., ACS applied materials & interfaces, 2013, 5, 4026–4030.
47 R. Anderson et al., The Journal of Physical Chemistry C, 2009, 113, 12602–12607.
48 P. Boutron et al., The Journal of Physical Chemistry, 1978, 68, 5032–5041.
49 A. D. Potts et al., The Journal of Physical Chemistry, 1965, 69, 996–1000.

View Article Online
DOI: 10.1039/C9MH00859D

Figure 1 | A thin lubricating ethanol layer for reducing ice adhesion strength. (a) Atomistic model of an ethanol lubricating layer at the ice-solid interface. The ice is shown in white and the carbon-based substrate is in green. Periodic boundary of the system is shown in green. Directions of pulling and shearing force applied on the ice to probe ice adhesion (σ) and shearing (τ) stresses are indicated by red arrows. (b) Ice adhesion stress, σ, on the same substrate with an ethanol layers of 0, 1 and 2 nm in thickness. (c) Ice shearing stresses, τ, with an ethanol layer of 0, 1 and 2 nm in thickness at -18 ℃. (d) Ice shearing stress, τ, on ethanol layer of 2 nm in thickness at various temperature.

Figure 2 | Schematic illustration of the strategies of generating a liquid layer at the ice-substrate interface. (a) Two strategies of create icephobic LLGs, namely packing ethanol inside substrate (left panel) and storing replenishable ethanol below substrate (right panel). **(b)** The mechanism of generating a liquid ethanol layer at the ice-substrate interface. **(c)** Fabricating method of the LLG 1: mixing ethanol with silicone rubber that quickly cured in room temperature, then ethanol will be packed inside the substrate body after curing. The optical image on the right shows the top view of LLG 1 (with 20 vol% ethanol), the small bubbles are the ethanol droplets inside the body. **(d)** Fabricating method of the LLG 2: Replica method for producing sub-pores for storage of ethanol below the surface. The SEM image on the right shows the side view of LLG 2 (distance between neighbor holes is 15 μm). Well arranged small holes can be observed on the bottom surface.

Figure 3 | Icephobicity of LLGs fabricated by packing ethanol inside the substrate. (a) Comparison of the adhesion of ice cube on the LLG 1 surface (left) and the same surface after fully removing the ethanol (right) at -18 ℃. **(b)** Diffusivity of dyestuff on the surfaces of ice cubes that peeled off from LLG 1 (left) and the one after removing ethanol (right). The ^{1}H NMR spectra (bottom) of liquid layer on the adhesion side of the ice cube (the area marked with red circle). **(c)** Comparison of ice adhesion strength on the LLG 1 with various ethanol content and the same surfaces after ethanol removal at -18 ℃. **(d)** The weight loss of the LLG 1 as functions of time at room temperature. **(e)** The weight loss of the LLGs as functions of time at -20 ℃.

Figure 4 | Icephobicity of LLGs with replenishable ethanol capacity. (a)-(c) Optical images showing silicon wafers with pillars of different density, the distance between neighbor pillars were 15 μm, 20 μm and 30 μm, respectively. **(d)-(f)** Scanning electron micrographs showing the hole morphologies of PDMS film fabricated on the silicon wafer in (a)-(c). **(g)** Comparison of ice adhesion on sample without infusing ethanol (left) and the LLG surface (right) at a temperature of -18 ℃. The distance between holes is 20 μm in both samples. **(h)** Ice adhesion strength on sample without ethanol (controlled PDMS) and LLG 2 with various hole density obtained at -18 ℃. **(i)** Liquid droplets on the surface of LLG (the area marked with red rectangle in g) after removing ice cube.

Figure 5 | Icephobicity of LLG 2 with coated nanoparticles and hydrophilic PVA. (a) Scanning electron micrographs showing homogenous nanoparticle coating on the top of LLGs. (b) Scanning electron micrographs of the cross-section of PVA coated LLG 2. The inset corresponds to the area highlighted by the red rectangle. **(c-d)** Comparison of ice adhesion strength on LLG 2 coated with nanoparticles and PVA at -18 ℃. **(e-f)** Comparison of ice adhesion strength on LLG 2 coated with nanoparticles and PVA at -60 ℃.

View Article Online DOI: 10.1039/C9MH00259D

View Article Online
DOI: 10.1039/C9MH00859D

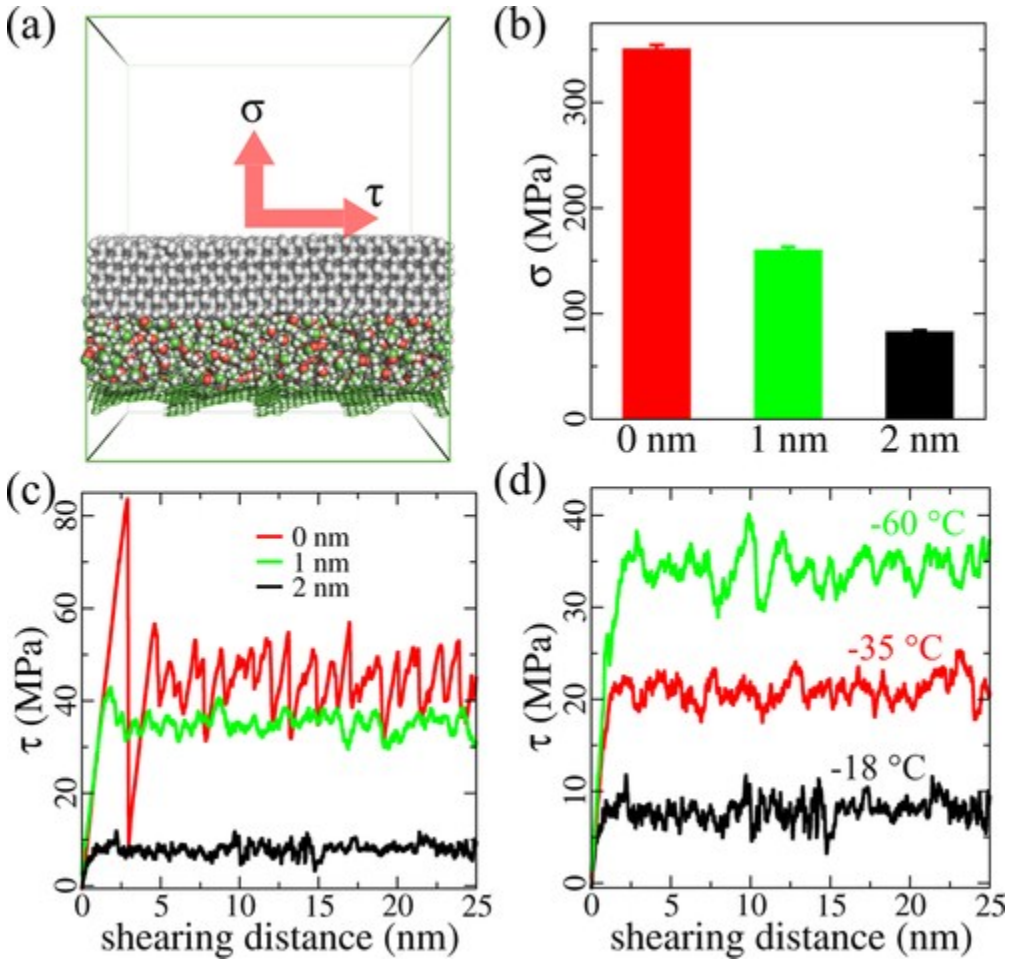

Figure 1 | A thin lubricating ethanol layer for reducing ice adhesion strength. (a) Atomistic model of an ethanol lubricating layer at the ice-solid interface. The ice is shown in white and the carbon-based substrate is in green. Periodic boundary of the system is shown in green. Directions of pulling and shearing force applied on the ice to probe ice adhesion (σ) and shearing (τ) stresses are indicated by red arrows. (b) Ice adhesion stress, σ, on the same substrate with an ethanol layers of 0, 1 and 2 nm in thickness. (c) Ice shearing stresses, τ, with an ethanol layer of 0, 1 and 2 nm in thickness at -18 ℃. (d) Ice shearing stress, τ, on ethanol layer of 2 nm in thickness at various temperature.

42x40mm (300 x 300 DPI)

View Article Online
DOI: 10.1039/C9MH00859D

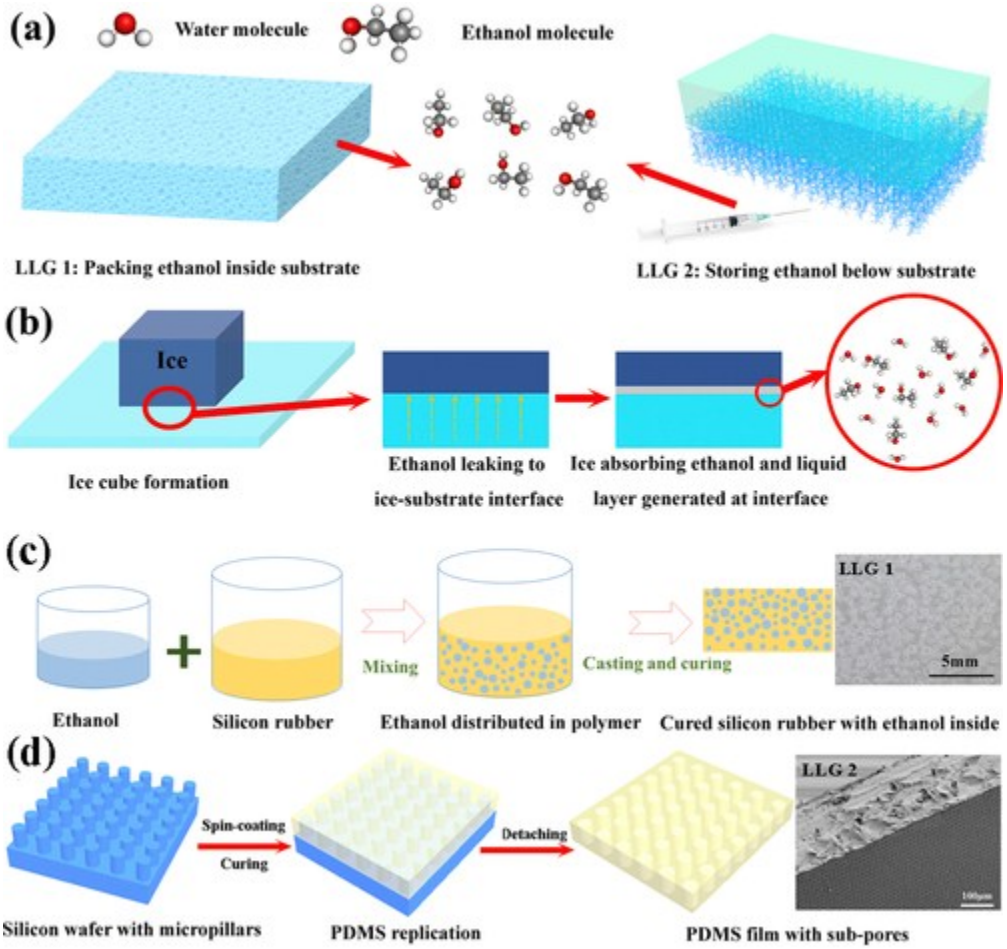

Caption : Figure 2 | Schematic illustration of the strategies of generating a liquid layer at the ice-substrate interface. (a) Two strategies of create icephobic LLGs, namely packing ethanol inside substrate (left panel) and storing replenishable ethanol below substrate (right panel). (b) The mechanism of generating a liquid ethanol layer at the ice-substrate interface. (c) Fabricating method of the LLG 1: mixing ethanol with silicone rubber that quickly cured in room temperature, then ethanol will be packed inside the substrate body after curing. The optical image on the right shows the top view of LLG 1 (with 20 vol% ethanol), the small bubbles are the ethanol droplets inside the body. (d) Fabricating method of the LLG 2: Replica method for producing sub-pores for storage of ethanol below the surface. The SEM image on the right shows the side view of LLG 2 (distance between neighbor holes is 15 μm). Well arranged small holes can be observed on the bottom surface.

42x40mm (300 x 300 DPI)

View Article Online
DOI: 10.1039/C9MH00859D

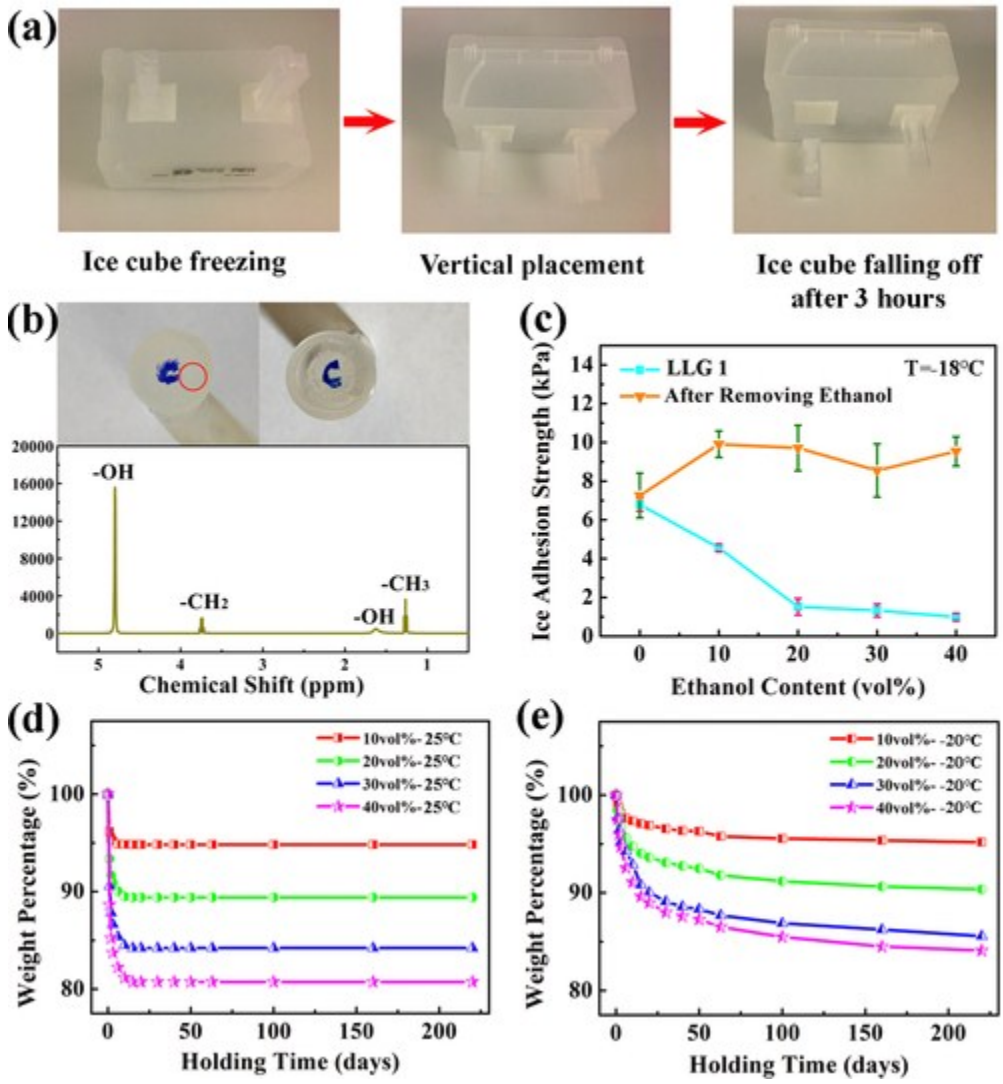

Figure 3 | Icephobicity of LLGs fabricated by packing ethanol inside the substrate. (a) Comparison of the adhesion of ice cube on the LLG 1 surface (left) and the same surface after fully removing the ethanol (right) at -18 ℃. (b) Diffusivity of dyestuff on the surfaces of ice cubes that peeled off from LLG 1 (left) and the one after removing ethanol (right). The 1H NMR spectra (bottom) of liquid layer on the adhesion side of the ice cube (the area marked with red circle). (c) Comparison of ice adhesion strength on the LLG 1 with various ethanol content and the same surfaces after ethanol removal at -18 ℃. (d) The weight loss of the LLG 1 as functions of time at room temperature. (e) The weight loss of the LLGs as functions of time at -20 ℃.

42x45mm (300 x 300 DPI)

View Article Online
DOI: 10.1039/C9MH00859D

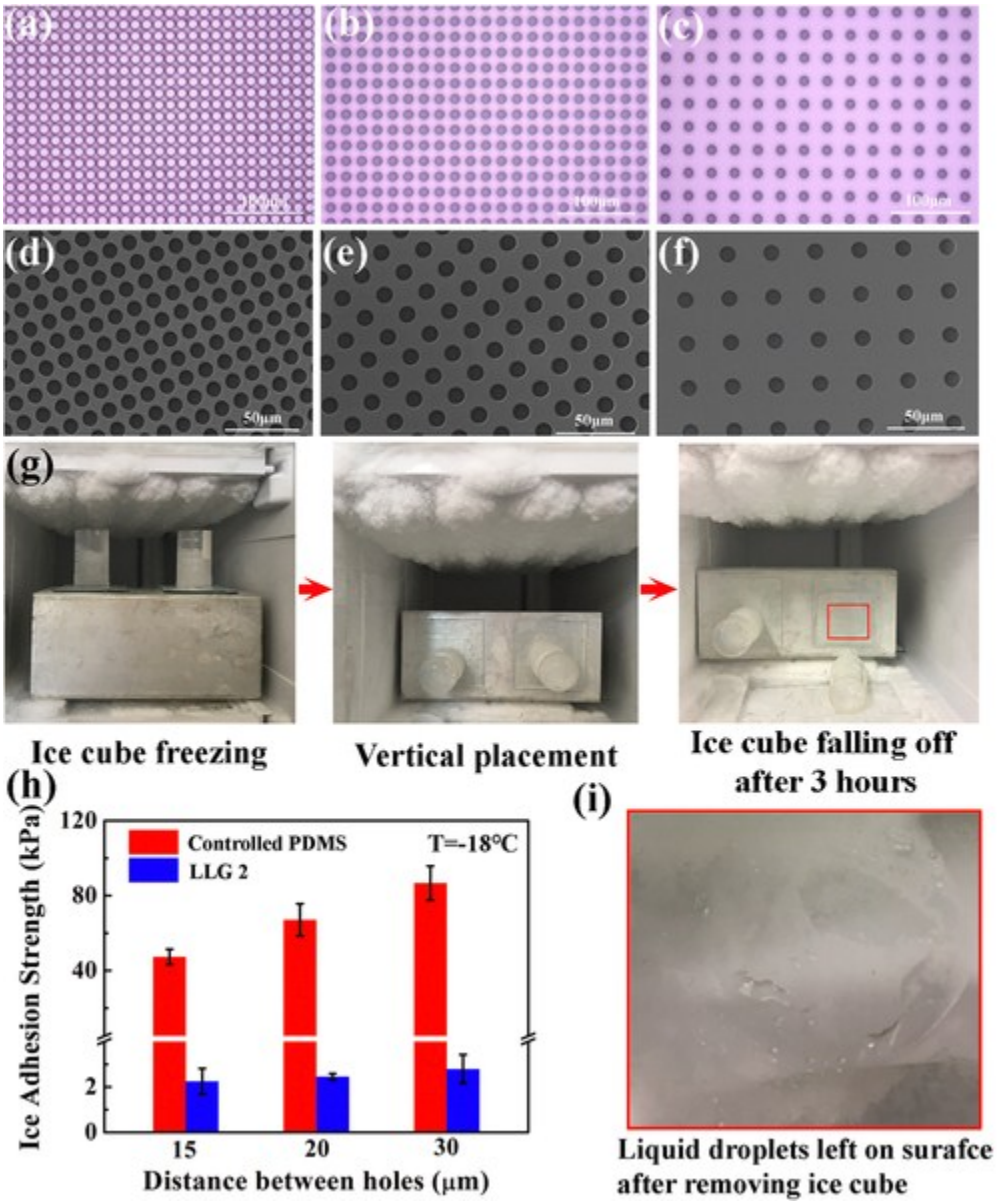

Figure 4 | Icephobicity of LLGs with replenishable ethanol capacity. (a)-(c) Optical images showing silicon wafers with pillars of different density, the distance between neighbor pillars were 15 μm, 20 μm and 30 μm, respectively. (d)-(f) Scanning electron micrographs showing the hole morphologies of PDMS film fabricated on the silicon wafer in (a)-(c). (g) Comparison of ice adhesion on sample without infusing ethanol (left) and the LLG surface (right) at a temperature of -18 ℃. The distance between holes is 20 μm in both samples. (h) Ice adhesion strength on sample without ethanol (controlled PDMS) and LLG 2 with various hole density obtained at -18 ℃. (i) Liquid droplets on the surface of LLG (the area marked with red rectangle in g) after removing ice cube.

42x50mm (300 x 300 DPI)

View Article Online
DOI: 10.1039/C9MH00859D

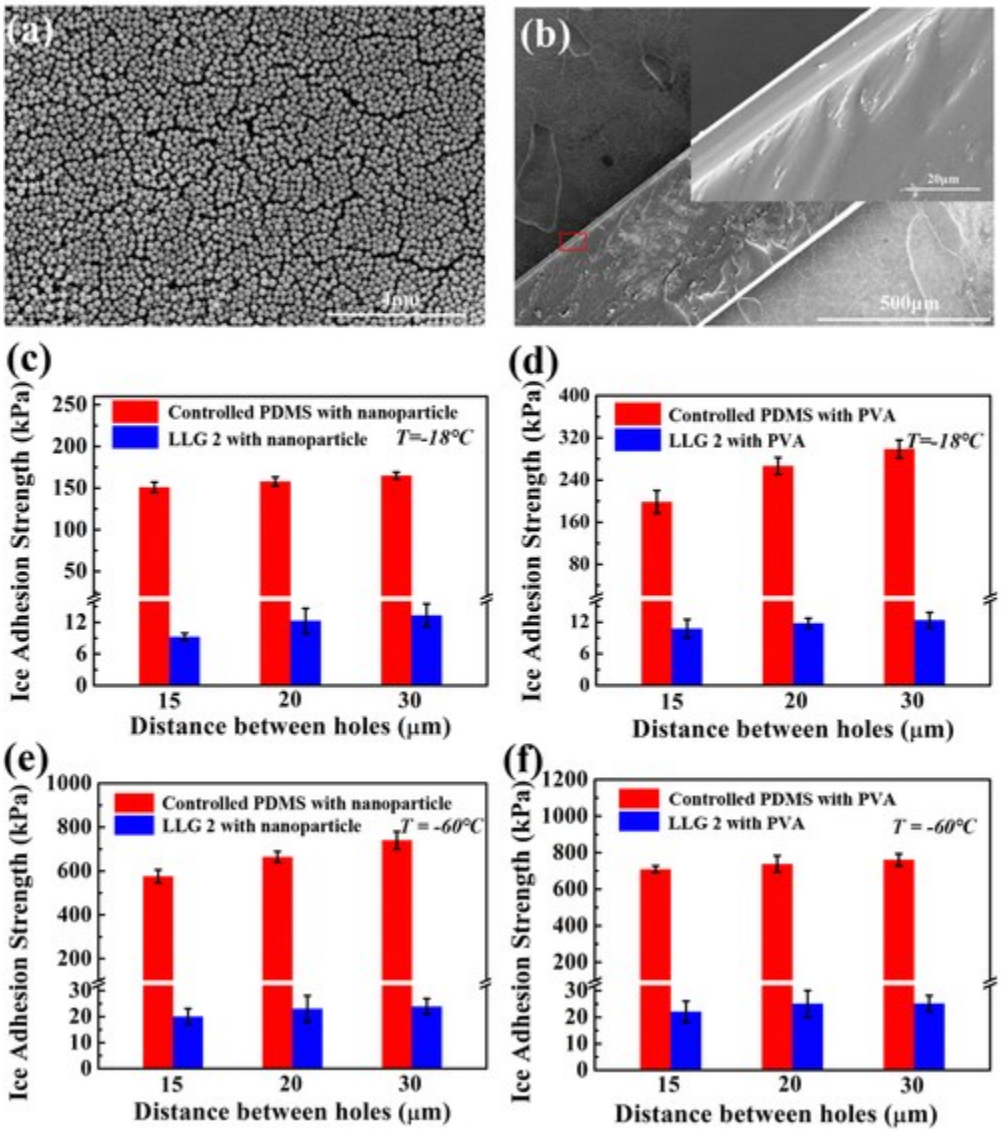

Figure 5 | Icephobicity of LLG 2 with coated nanoparticles and hydrophilic PVA. (a) Scanning electron micrographs showing homogenous nanoparticle coating on the top of LLGs. (b) Scanning electron micrographs of the cross-section of PVA coated LLG 2. The inset corresponds to the area highlighted by the red rectangle. (c-d) Comparison of ice adhesion strength on LLG 2 coated with nanoparticles and PVA at -18 ℃. (e-f) Comparison of ice adhesion strength on LLG 2 coated with nanoparticles and PVA at -60 ℃.

42x48mm (300 x 300 DPI)

View Article Online
DOI: 10.1039/C9MH00859D

Conceptual Insights Statement

State-of-the-art icephobic surfaces mainly rely on static solid-solid ice-substrate contact, which fail at low temperature reaching a threshold of around -50°C. New strategy for anti-icing at such low temperature is missing. Dynamic anti-icing surfaces, which can melt ice at or change the ice-substrate interfaces from solid to liquid phase after the formation of ice serves as a viable alternative. In the current study, durable polymeric materials, termed liquid layer generators, were design and fabricated targeting low ice adhesion strength at unprecedentedly low temperature. The liquid layer generators were able to constantly release interfacial ethanol for maximally 593 days, which dynamically convert ice contact from firm solid-solid to weak solid-liquid-solid mode, and demonstrated super low ice adhesion strength of ~1kPa. By introducing porous layer below substrate, interfacial liquid layer can be controlled by replenishable ethanol. The liquid layer generator can also overcome problems of surface roughness and hydrophilicity that fail other icephobic surfaces. At extremely low temperature of -60°C, the liquid layer generators maintained low ice adhesion strength (22.1~25.2 kPa), showing encouraging potential for practical arctic anti-icing utilization.